A Comparative Study on Depth of Penetration Measurements in Diagnostic Ultrasounds Through the Adaptive SNR Threshold Method

Giorgia Fiori, *Member, IEEE*, Fabio Fuiano, Maurizio Schmid, *Senior Member, IEEE*, Silvia Conforto, *Member, IEEE*, Salvatore A. Sciuto, *Member, IEEE*, and Andrea Scorza

***Abstract*— Depth of penetration (DOP) has been investigated in the scientific literature as an informative parameter able to monitor over time both the sensitivity and the general performance of ultrasound (US) diagnostic systems. In common practice, this parameter may suffer from operator-related errors due to its visual assessment. Different image analysis algorithms have been proposed in the literature to address this issue. In this regard, this work evaluates the adaptive SNR threshold method (AdSTM) on six US diagnostic systems equipped with three US probe models, operating at four frequencies. Data were collected from a US phantom with two distinct zones with different attenuation coefficients. The AdSTM results were compared to the outcomes provided by the naked eye method (NEM), which was performed by five non-medical observers. Despite the small population sample of observers, the obtained results were generally consistent across methods, and suggest the implementation of a calibration procedure for AdSTM, and more extensive testing.**

***Index Terms*— Adaptive threshold, attenuation, naked eye method (NEM), penetration depth, quality controls (QCs), ultrasonic imaging.**

I. Introduction

QUALITY assessment is a hot topic in the scientific community these days [1], [2], [3], [4], [5]. For medical ultrasound (US), depth of penetration (DOP) is one of the most influential parameters in quality controls (QCs), as it is regarded as a useful tool for obtaining valuable information about the progressive deterioration of US system performance over time [6]. DOP is also closely related to sensitivity [7], which is an important metrological characteristic for determining the quality of a US system. DOP has been defined in numerous studies [8], [9], [10], [11] as the highest depth value at which US signals can still be distinguished from electronic noise due to the scattering phenomenon that occurs when echoes pass through a tissue-mimicking material (TMM). Currently, when periodic QCs are performed, DOP is retrieved by eye on the US system display [2], [12], [13] as the depth level beyond which a clear distinction of the displayed US speckle, due to TMM, is prevented by the presence of background electronic noise [12]. Because of the dependency on the patient, the phantom, and the operator, such a method is unsuitable for guaranteeing the repeatability of DOP measurements, although US settings and environmental conditions, (e.g., light) are maintained throughout the measurement procedure [9]. As a result, offline image analysis methods have been proposed in the literature [6], [10], [11], [14] to address the issues related to the intrinsic subjectivity of visual tests. Nevertheless, despite the solutions deployed, the scientific community is still waiting for a globally shared standard on US equipment quality assessment obtained through this parameter. To date, the most promising approach for DOP assessment, recommended as a standard reference method in [6], is based on the estimation of signal-to-noise ratio (SNR) for increasing depths in US images [15], [16], [17]. DOP is defined as the depth at which the estimated SNR value exceeds a predetermined threshold. In any case, many of the aforementioned SNR-based algorithms rely on ambiguous criteria for threshold determination [15], [18] or suffer from operator dependence uncertainty [12]. The adaptive SNR threshold method (AdSTM), a novel image analysis SNR-based method for DOP assessment, was recently introduced to address these limitations. It is based on automatic threshold determination, thus improving the method in [14], and as shown in the previous preliminary studies [19], [20], it has the advantage of increasing the reliability and reproducibility of the results. The goal of this study is thus to test the AdSTM across a variety of US diagnostic systems and configurations available on the market, including different probe models, and to analyze the DOP variation in response to different probe operating frequencies at distinct levels of medium attenuation. DOP uncertainty was assessed using a series of Monte Carlo simulations (MCSs). Finally, the obtained results were compared to the naked eye method's (NEM) scores of independent observers.

Manuscript received 19 October 2022; revised 30 December 2022; accepted 4 February 2023. Date of publication 2 March 2023; date of current version 13 March 2023. The Associate Editor coordinating the review process was Dr. Yixin Ma. *(Corresponding author: Giorgia Fiori.)*

The authors are with the Department of Industrial, Electronic and Mechanical Engineering, Roma Tre University, 00146 Rome, Italy (e-mail: giorgia.fiori@uniroma3.it; fabio.fuiano@uniroma3.it; maurizio.schmid@uniroma3.it; silvia.conforto@uniroma3.it; salvatore.sciuto@uniroma3.it; andrea.scorza@uniroma3.it).

Digital Object Identifier 10.1109/TIM.2023.3250309

II. Materials and Methods

A. Adaptive SNR Threshold Method

As described in [19] and [21], the AdSTM image analysis SNR-based method for DOP assessment (Fig. 1) was developed by processing phantom and in-air clips (the latter

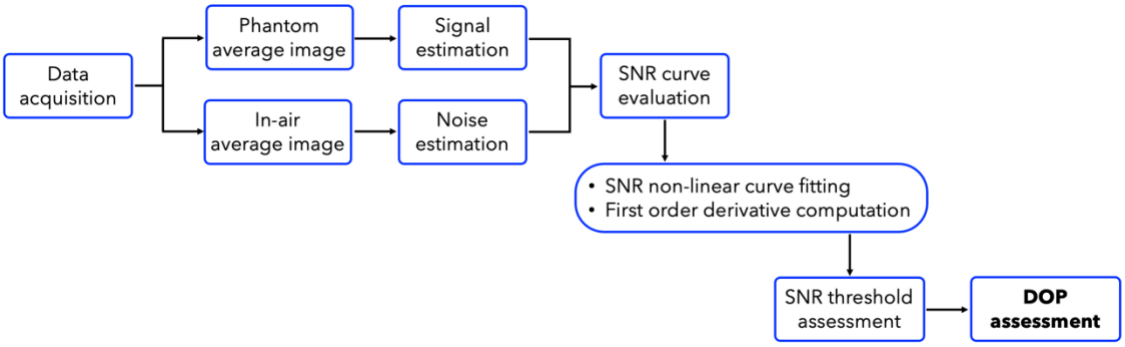

Fig. 1. Block diagram of the main processing steps of the AdSTM for DOP assessment.

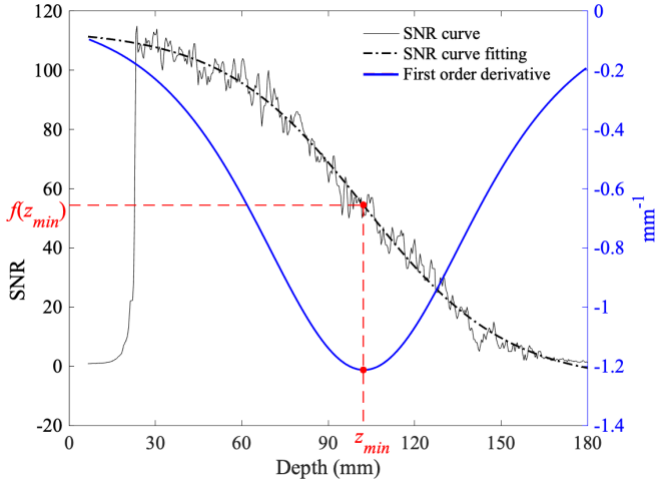

Fig. 2. Example of the estimation of an SNR curve, sigmoidal fitting, and its corresponding first-order derivative.

obtained by decoupling the probe from the phantom surface). The method, implemented through a custom-written MATLAB function, post-processes video clips taken from phantom and air observations by averaging N consecutive frames to produce two average images (I_{ph} and I_{air}). Then, a rectangular region of interest (ROI) of fixed width is automatically drawn from I_{ph} and I_{air} to compute the signal and the noise contributions, respectively [19]. The SNR curve is then estimated as a function of depth z, and the threshold th_{SNR} is computed as follows:

$$\text{th}_{\text{SNR}} = \frac{\Delta g \cdot \alpha}{L_s} \tag{1}$$

where Δg is the smallest gray level difference perceivable by the human eye [19], [21], [22], L_s is the maximum luminance level, and α is the maximum sensitivity of the US system. The latter is obtained by applying the following steps [19]:

1) Determination of the sigmoidal function $f(z)$ through SNR curve non-linear fitting.
2) Computation of the first-order derivative of $f(z)$ is needed to locate the depth $z_{\min}$ (Fig. 2) corresponding to its minimum value $\alpha = f(z_{\min})$.

The DOP is then automatically calculated as the depth value where the threshold th_{SNR} intersects the SNR curve.

AdSTM robustness was tested in this study by comparing the obtained values to those determined by NEM, i.e., through visual examination of five separate observers (excluding people with medical expertise during testing). The observers' judgment was independently performed on the average image I_{ph} in a similar fashion to [19], through a further in-house MATLAB function, by preserving the same environment lighting and setting conditions. A sixfold repetition was chosen to test both intra- and interindividual variability of the observers involved in this study.

B. Experimental Setup

A multi-purpose, multi-tissue US phantom (CIRS, Model 040GSE) [23] was used to collect the phantom clips. This reference device is constituted by two attenuation zones (0.70 and 0.50 dB·cm^{-1}·MHz^{-1}). Data were acquired from six intermediate technology level US diagnostic systems equipped with three US probe models (linear, phased, and convex array) at both attenuation zones. Each probe was placed on the phantom scanning surface where the speckle background is visible, avoiding grayscale targets, anechoic stepped cylinders, and nylon wires embedded in the phantom. To maximize US energy transmission, a coupling gel was used, and the probes were held in place by a holder.

Both the phantom and in-air clips were collected under the same raw scanning settings (see Table I). This configuration ensures that all the US systems operate under the same conditions, therefore allowing proper outcome comparison. The AdSTM was used to post-process all the acquired video clips. In particular, the average images were obtained by averaging $N = 15$ consecutive frames (Fig. 3). After that, an automatically driven mask-like crop on I_{ph} and I_{air} allowed excluding from the images the superimposed setting details [19]. Furthermore, based on the considerations discussed in [19], an accurate estimation of DOP can be performed by setting an ROI width of 30 px (3−5 mm for the linear array probe, 7−11 mm for the phased one, and 8−11 mm for the convex one).

III. Monte Carlo Simulation

MCS was chosen for AdSTM testing, as several studies in the literature [24], [25], [26], [27], [28] testify that it is a

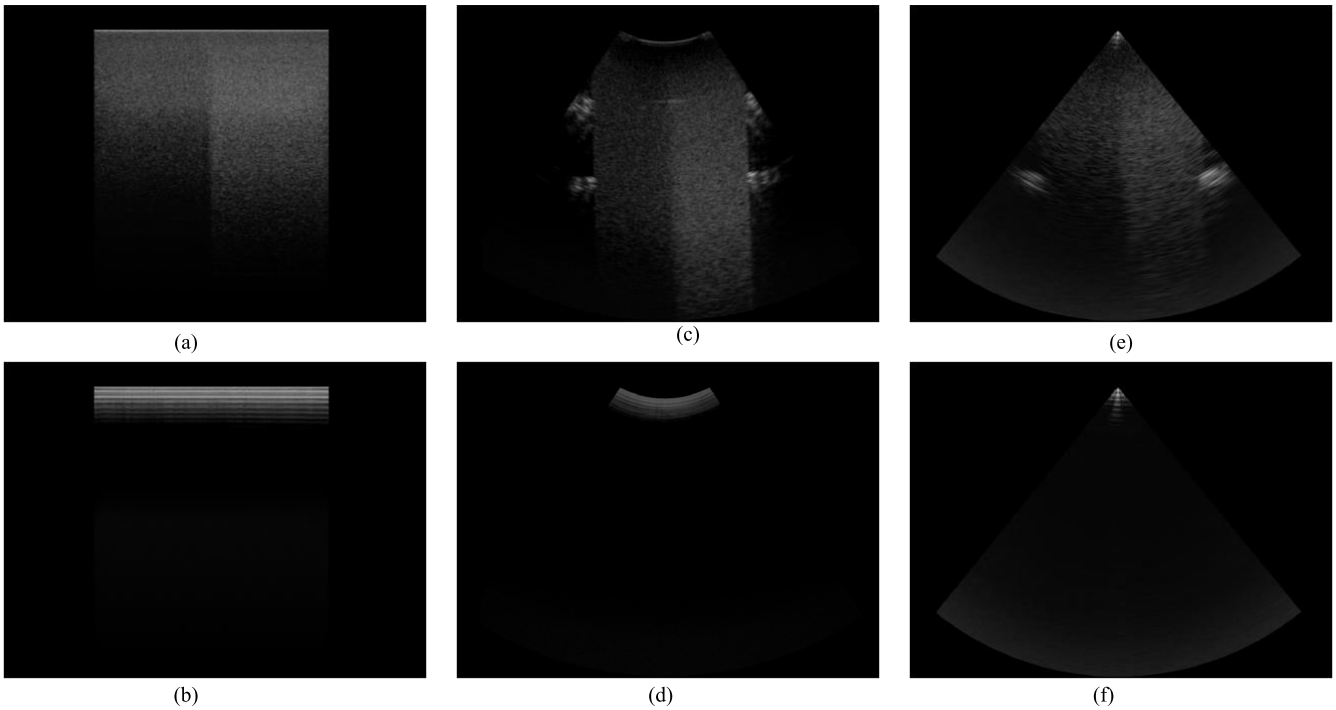

Fig. 3. Examples of average images obtained from (a), (c), and (e) phantom, (b), (d), and (f) in-air clips acquired with (a) and (b) linear, (c) and (d) phased, and (e) and (f) convex array probe operating at medium frequency.

TABLE I
US RAW SYSTEM SETTINGS

Parameter		Setting
Nominal frequency range (MHz)	L	2-18
	P	1-5
	C	1-8
Field of view range (mm)	L	70-120
	P	180-191
	C	180-190
Time Gain Compensation		Sliding cursors aligned in middle position
Dynamic range		Maximum
Persistence		Minimum
Edge enhancement		Minimum
Post-processing		Linear
Power transmission		Maximum

L = linear array probe; P = phased array probe; C = convex array probe. The US systems in the tests are the following: Acuson S2000 (Siemens), HS60 (Samsung), Affiniti 70 (Philips), Arietta V70a (Hitachi), Versana Premier (GE) and MyLab X8 (Esaote).

TABLE II
MCS SETTINGS FOR THE UNCERTAINTY ESTIMATION OF BOTH THE SNR THRESHOLD AND DOP OUTCOMES

Parameter	Distribution	Mean ± SD
ROI width (w)	uniform	30 ± 1 px
ROI shift (s)	uniform	$s_0 \pm 2$ px

SD = standard deviation; s_0 is the ROI shift starting point.

powerful tool for evaluating the uncertainty of software-based measurements and the extent of their robustness.

To simulate the uncertainty caused by operator drawing, the ROI width w and shift s (both expressed in terms of the number of pixels) were varied within a uniform distribution.

A first series of MCSs ($7{\cdot}10^3$ cycles, to reduce computational burden) was run with w and s as input distributions (see Table II), obtaining the th_{SNR} distributions as output. It is worth noting that the SNR threshold is an adimensional parameter whose value depends on the probe used but it does not seem to be relevantly affected by the distributions in Table II. As a result, different mean and standard deviation (SD) values can be obtained depending on the probe type. These variations are due to the different SNR curve characteristics of the US images acquired for each US probe-system pair. Subsequently, DOP histograms were computed as the result of a further MCSs series iterative execution (10^5 cycles) with th_{SNR} data from the previous simulations (listed in Tables III and IV) as inputs.

IV. RESULTS

Tables III and IV present DOP results from three different US probes tested at four operating frequencies, for all the six US systems, obtained by the AdSTM and the NEM, in correspondence with the two phantom attenuation zones. AdSTM uncertainties δ_{AdSTM} were computed by combining the repeatability uncertainties, from 2.5 and 97.5 MCS distribution percentiles, and those due to probe position on the phantom scanning surface, whose values were estimated in [29]. NEM uncertainties δ_{NEM} were estimated as the square root of the mean squared error of the data obtained through the visual examinations by considering a coverage factor of 2. One-way ANOVA ($p < 0.3$ for the lower attenuation zone and $p < 0.1$ for the higher attenuation zone) was then performed on NEM uncertainties to check for intra- and inter-observer variability.

TABLE III
DOP MEASUREMENTS FOR DIAGNOSTIC SYSTEMS I–III: RESULTS COMPARISON FOR THREE US PROBES ACCORDING TO THE OPERATING FREQUENCY

US system and probe		FOV (mm)	f_{probe}	0.70 dB·cm^{-1}·MHz^{-1}						0.50 dB·cm^{-1}·MHz^{-1}					
				AdSTM				NEM		AdSTM				NEM	
				th_{SNR}		DOP (mm)	$\delta_{AdSTM\%}$	DOP (mm)	$\delta_{NEM\%}$	th_{SNR}		DOP (mm)	$\delta_{AdSTM\%}$	DOP (mm)	$\delta_{NEM\%}$
Ultrasound System I	L	70	f_{min}	2.62 ± 0.01	u	44 ± 2	± 2.9%	41 ± 3	± 4%	2.72 ± 0.02	u	61 ± 2	± 2.9%	58 ± 2	± 2.9%
			f_{med}	3.7 ± 0.1	t	46 ± 2	± 2.9%	39 ± 2	± 2.9%	2.76 ± 0.02	t	62 ± 2	± 2.9%	61 ± 8	± 11%
			f_{max}	2.44 ± 0.01	u	49 ± 2	± 2.9%	49 ± 2	± 2.9%	—		≥ FOV[a]		67 ± 3[b]	± 4%
			f_h	2.94 ± 0.08	u	39 ± 2	± 2.9%	35 ± 2	± 2.9%	3.81 ± 0.02	g	51 ± 2	± 2.9%	51 ± 2	± 2.9%
	P	180	f_{min}	2.08 ± 0.07	u	150 ± 3	± 1.7%	136 ± 7	± 4%	—		≥ FOV[a]		180 ± 2[b]	± 1.1%
			f_{med}	1.94 ± 0.04	t	124 ± 2	± 1.1%	113 ± 10	± 6%	—		≥ FOV[a]		180 ± 2[b]	± 1.1%
			f_{max}	Probe frequency not available											
			f_h	2.32 ± 0.01	g	129 ± 5	± 2.8%	116 ± 5	± 2.8%	—		≥ FOV[a]		176 ± 10[b]	± 6%
	C	180	f_{min}	1.93 ± 0.02	g	159 ± 6	± 3%	150 ± 7	± 4%	—		≥ FOV[a]		≥ FOV	
			f_{med}	2.26 ± 0.02	t	151 ± 6	± 3%	139 ± 6	± 3%	—		≥ FOV[a]		≥ FOV	
			f_{max}	4.0 ± 0.2	u	160 ± 3	± 1.7%	136 ± 5	± 2.8%	—		≥ FOV[a]		≥ FOV	
			f_h	8.49 ± 0.07	t	157 ± 3	± 1.7%	119 ± 10	± 6%	—		≥ FOV[a]		176 ± 7[b]	± 4%
Ultrasound System II	L	70	f_{min}	2.37 ± 0.02	g	41 ± 2	± 2.9%	39 ± 3	± 4%	2.55 ± 0.15	u	61 ± 2	± 2.9%	58 ± 2	± 2.9%
			f_{med}	1.91 ± 0.04	u	36 ± 3	± 4%	36 ± 2	± 2.9%	1.98 ± 0.04	u	51 ± 3	± 4%	49 ± 3	± 4%
			f_{max}	1.17 ± 0.03	u	38 ± 3	± 4%	34 ± 3	± 4%	3.3 ± 0.2	u	46 ± 3	± 4%	44 ± 3	± 4%
			f_h	1.00 ± 0.01	u	29 ± 2	± 2.9%	24 ± 2	± 2.9%	1.10 ± 0.01	u	38 ± 2	± 2.9%	34 ± 2	± 2.9%
	P	180	f_{min}	Data not available											
			f_{med}	1.10 ± 0.02	t	101 ± 5	± 2.8%	100 ± 12	± 7%	1.33 ± 0.01	u	161 ± 5	± 2.8%	152 ± 11	± 6%
			f_{max}	Data not available											
			f_h	1.09 ± 0.01	u	98 ± 4	± 2.2%	86 ± 6	± 3%	1.25 ± 0.01	u	124 ± 3	± 1.7%	123 ± 7	± 4%
	C	180	f_{min}	1.79 ± 0.01	g	166 ± 8	± 4%	143 ± 21	± 12%	—		≥ FOV[a]		≥ FOV	
			f_{med}	1.52 ± 0.04	u	152 ± 3	± 1.7%	130 ± 8	± 4%	—		≥ FOV[a]		178 ± 2[b]	± 1.1%
			f_{max}	1.73 ± 0.02	t	140 ± 3	± 1.7%	131 ± 6	± 3%	—		≥ FOV[a]		172 ± 11[b]	± 6%
			f_h	1.8 ± 0.1	u	113 ± 4	± 2.2%	81 ± 9	± 5%	1.07 ± 0.04	u	161 ± 6	± 3%	151 ± 6	± 3%
Ultrasound System III	L	70	f_{min}	1.57 ± 0.04	t	43 ± 2	± 2.9%	40 ± 2	± 2.9%	2.79 ± 0.03	u	55 ± 2	± 2.9%	54 ± 3	± 4%
			f_{med}	1.38 ± 0.03	t	43 ± 2	± 2.9%	39 ± 2	± 2.9%	2.49 ± 0.05	u	53 ± 3	± 4%	51 ± 2	± 2.9%
			f_{max}	1.31 ± 0.03	g	42 ± 2	± 2.9%	37 ± 2	± 2.9%	3.38 ± 0.06	g	51 ± 2	± 2.9%	49 ± 2	± 2.9%
			f_h	1.09 ± 0.05	t	42 ± 2	± 2.9%	36 ± 2	± 2.9%	2.90 ± 0.07	u	49 ± 2	± 2.9%	49 ± 2	± 2.9%
	P	180	f_{min}	1.79 ± 0.02	t	126 ± 4	± 2.2%	108 ± 7	± 4%	4.67 ± 0.05	g	151 ± 6	± 3%	147 ± 8	± 4%
			f_{med}	1.76 ± 0.06	t	120 ± 2	± 1.1%	103 ± 7	± 4%	3.49 ± 0.04	t	148 ± 6	± 3%	140 ± 10	± 6%
			f_{max}	1.41 ± 0.05	t	124 ± 2	± 1.1%	101 ± 10	± 6%	4.00 ± 0.06	u	141 ± 2	± 1.1%	139 ± 9	± 5%
			f_h	2.75 ± 0.02	g	99 ± 5	± 2.8%	85 ± 5	± 2.8%	6.5 ± 0.1	u	118 ± 3	± 1.7%	117 ± 7	± 4%
	C	180	f_{min}	0.70 ± 0.01	u	101 ± 2	± 1.1%	84 ± 5	± 2.8%	1.44 ± 0.01	u	129 ± 2	± 1.1%	116 ± 5	± 2.8%
			f_{med}	0.49 ± 0.04	t	99 ± 2	± 1.1%	79 ± 5	± 2.8%	1.09 ± 0.02	u	117 ± 2	± 1.1%	107 ± 5	± 2.8%
			f_{max}	0.41 ± 0.01	t	93 ± 3	± 1.7%	79 ± 8	± 4%	0.92 ± 0.02	t	111 ± 2	± 1.1%	101 ± 5	± 2.8%
			f_h	0.23 ± 0.02	g	81 ± 4	± 2.2%	53 ± 11	± 6%	0.97 ± 0.03	u	109 ± 2	± 1.1%	97 ± 5	± 2.8%

FOV = Field of View; L = linear array probe; P = phased array probe; C = convex array probe. f_h is the maximum harmonic probe frequency; g = gaussian distribution; t = triangular distribution; u = uniform distribution. Results are expressed in terms of mean ± uncertainty (uncertainty δ_{AdSTM} and δ_{NEM} for AdSTM and NEM, respectively). Alongside DOP results, the percentage error values with respect to the FOV are reported and computed as $\delta_{AdSTM\%} = (100 \cdot \delta_{AdSTM} / FOV)$ and $\delta_{NEM\%} = (100 \cdot \delta_{NEM} / FOV)$, respectively; (a) AdSTM does not provide a SNR threshold value when DOP value is greater or equal to the FOV; (b) A no negligible number of tests provided a DOP value above the FOV.

In the cases marked with (*) in Tables III and IV, the AdSTM did not yield an SNR threshold because the DOP value is greater than or equal to the field of view (FOV). This occurs because of the US probe sensitivity combined with the limited phantom depth and the low attenuation coefficient. Nevertheless, the AdSTM and the NEM data in such cases are always consistent, therefore indicating that the automatic method provides accurate information also in such extreme cases.

The percentage error values with respect to the FOV ($\delta_{AdSTM\%}$ and $\delta_{NEM\%}$ for the AdSTM and the NEM, respectively) were computed from DOP uncertainties with a procedure similar to [19] and [20] as follows:

$$\delta_{AdSTM\%} = \frac{\delta_{AdSTM}}{FOV} \cdot 100 \tag{2}$$

$$\delta_{NEM\%} = \frac{\delta_{NEM}}{FOV} \cdot 100. \tag{3}$$

The mean percentage errors in correspondence of 0.70 and 0.50 dB·cm^{-1}·MHz^{-1} attenuation zones are 2.2% and 2.5%, respectively, for the AdSTM, while 3.9% and 4.2%, respectively, for the NEM. No significant difference was found between the percentage error values retrieved for the two different attenuations. These results confirm that AdSTM

TABLE IV

DOP MEASUREMENTS FOR DIAGNOSTIC SYSTEMS IV–VI: RESULTS COMPARISON FOR THREE US PROBES ACCORDING TO THE OPERATING FREQUENCY

US system and probe		FOV (mm)	f_{probe}	0.70 dB·cm^{-1}·MHz^{-1}						0.50 dB·cm^{-1}·MHz^{-1}					
				AdSTM				NEM		AdSTM				NEM	
				th_{SNR}		DOP (mm)	$\delta_{AdSTM\%}$	DOP (mm)	$\delta_{NEM\%}$	th_{SNR}		DOP (mm)	$\delta_{AdSTM\%}$	DOP (mm)	$\delta_{NEM\%}$
Ultrasound System IV	L	120	f_{min}	0.51 ± 0.02	u	58 ± 5	± 4%	39 ± 8	± 7%	0.61 ± 0.05	u	79 ± 2	± 1.7%	70 ± 3	± 2.5%
		74	f_{med}	0.54 ± 0.02	u	43 ± 2	± 2.7%	35 ± 3	± 4%	2.77 ± 0.02	u	56 ± 2	± 2.7%	52 ± 4	± 5%
			f_{max}	1.35 ± 0.01	t	34 ± 4	± 5%	29 ± 3	± 4%	1.56 ± 0.01	u	49 ± 2	± 2.7%	45 ± 3	± 4%
			f_h	0.29 ± 0.02	g	24 ± 2	± 2.7%	19 ± 2	± 2.7%	0.54 ± 0.01	u	38 ± 2	± 2.7%	31 ± 3	± 4%
	P	191	f_{min}	2.22 ± 0.03	u	149 ± 2	± 1.0%	146 ± 11	± 6%	—		≥ FOV[a]		186 ± 5[b]	± 2.6%
			f_{med}	1.55 ± 0.08	u	138 ± 6	± 3%	121 ± 8	± 4%	3.8 ± 0.1	u	177 ± 2	± 1.0%	164 ± 10	± 5%
			f_{max}	1.44 ± 0.06	u	139 ± 3	± 1.6%	119 ± 10	± 5%	2.18 ± 0.05	g	167 ± 3	± 1.6%	166 ± 13	± 7%
			f_h	0.72 ± 0.02	g	110 ± 2	± 1.0%	85 ± 6	± 3%	1.09 ± 0.02	u	144 ± 2	± 1.0%	120 ± 8	± 4%
	C	184	f_{min}	1.15 ± 0.02	u	142 ± 3	± 1.6%	110 ± 13	± 7%	3.32 ± 0.08	g	171 ± 5	± 2.7%	161 ± 23[b]	± 13%
			f_{med}	0.46 ± 0.01	t	107 ± 2	± 1.1%	71 ± 8	± 4%	0.70 ± 0.05	u	149 ± 5	± 2.7%	122 ± 5	± 2.7%
			f_{max}	0.42 ± 0.02	u	91 ± 2	± 1.1%	46 ± 11	± 6%	0.93 ± 0.03	g	134 ± 2	± 1.1%	100 ± 11	± 6%
			f_h	0.33 ± 0.02	u	96 ± 2	± 1.1%	51 ± 6	± 3%	0.52 ± 0.01	u	130 ± 5	± 2.7%	109 ± 7	± 4%
Ultrasound System V	L	90	f_{min}	1.04 ± 0.06	u	57 ± 2	± 2.2%	51 ± 3	± 3%	2.39 ± 0.03	g	70 ± 3	± 3%	70 ± 3	± 3%
			f_{med}	0.51 ± 0.04	u	48 ± 3	± 3%	45 ± 2	± 2.2%	1.55 ± 0.07	u	62 ± 2	± 2.2%	60 ± 2	± 2.2%
			f_{max}	0.6 ± 0.1	t	33 ± 5	± 6%	35 ± 5	± 6%	0.85 ± 0.03	g	57 ± 2	± 2.2%	54 ± 3	± 3%
			f_h	0.7 ± 0.1	u	21 ± 2	± 2.2%	16 ± 2	± 2.2%	0.81 ± 0.09	g	50 ± 2	± 2.2%	50 ± 2	± 2.2%
	P	180	f_{min}	1.33 ± 0.02	g	92 ± 2	± 1.1%	83 ± 4	± 2.2%	1.80 ± 0.01	u	124 ± 2	± 1.1%	120 ± 6	± 3%
			f_{med}	1.44 ± 0.03	u	105 ± 3	± 1.7%	88 ± 4	± 2.2%	1.88 ± 0.01	u	128 ± 3	± 1.7%	123 ± 5	± 2.8%
			f_{max}	1.13 ± 0.02	g	93 ± 2	± 1.1%	81 ± 3	± 1.7%	1.53 ± 0.02	g	118 ± 4	± 2.2%	111 ± 5	± 2.8%
			f_h	0.74 ± 0.05	u	86 ± 2	± 1.1%	77 ± 4	± 2.2%	1.33 ± 0.01	u	114 ± 3	± 1.7%	107 ± 5	± 2.8%
	C	190	f_{min}	0.63 ± 0.03	u	90 ± 5	± 2.6%	77 ± 8	± 4%	2.44 ± 0.05	g	168 ± 6	± 3%	162 ± 5	± 2.6%
			f_{med}	0.67 ± 0.05	u	85 ± 3	± 1.6%	75 ± 9	± 5%	1.23 ± 0.03	g	153 ± 2	± 1.1%	146 ± 6	± 3%
			f_{max}	0.22 ± 0.03	u	63 ± 2	± 1.1%	51 ± 5	± 2.6%	0.56 ± 0.07	u	130 ± 5	± 2.6%	118 ± 4	± 2.1%
			f_h	0.66 ± 0.02	g	58 ± 3	± 1.6%	50 ± 6	± 3%	0.80 ± 0.03	u	125 ± 5	± 2.6%	121 ± 7	± 4%
Ultrasound System VI	L	100	f_{min}	1.20 ± 0.06	u	41 ± 2	± 2.0%	35 ± 4	± 4%	2.8 ± 0.1	u	71 ± 6	± 6%	59 ± 6	± 6%
			f_{med}	1.16 ± 0.01	u	40 ± 2	± 2.0%	33 ± 3	± 3%	1.53 ± 0.01	u	73 ± 3	± 3%	57 ± 3	± 3%
			f_{max}	1.12 ± 0.04	u	22 ± 3	± 3%	20 ± 7	± 7%	1.31 ± 0.01	t	55 ± 5	± 5%	48 ± 4	± 4%
			f_h	1.13 ± 0.07	u	27 ± 4	± 4%	21 ± 3	± 3%	1.65 ± 0.06	t	35 ± 4	± 4%	30 ± 2	± 2.0%
	P	180	f_{min}	0.88 ± 0.01	u	130 ± 2	± 1.1%	109 ± 5	± 2.8%	—		≥ FOV[a]		162 ± 18[b]	± 10%
			f_{med}	0.88 ± 0.02	t	130 ± 2	± 1.1%	106 ± 6	± 3%	—		≥ FOV[a]		168 ± 12[b]	± 7%
			f_{max}	1.37 ± 0.06	u	117 ± 3	± 1.7%	94 ± 5	± 2.8%	5.54 ± 0.07	t	157 ± 3	± 1.7%	153 ± 27[b]	± 15%
			f_h	0.60 ± 0.02	t	77 ± 2	± 1.1%	61 ± 4	± 2.2%	1.5 ± 0.1	u	120 ± 4	± 2.2%	100 ± 5	± 2.8%
	C	180	f_{min}	0.60 ± 0.04	u	94 ± 2	± 1.1%	82 ± 6	± 3%	1.43 ± 0.04	g	153 ± 2	± 1.1%	138 ± 9	± 5%
			f_{med}	0.51 ± 0.01	u	99 ± 3	± 1.7%	78 ± 5	± 2.8%	2.70 ± 0.05	u	151 ± 6	± 3%	141 ± 13	± 7%
			f_{max}	0.32 ± 0.04	t	84 ± 3	± 1.7%	64 ± 6	± 3%	1.04 ± 0.02	t	138 ± 8	± 4%	122 ± 9	± 5%
			f_h	0.90 ± 0.01	u	47 ± 5	± 2.8%	32 ± 8	± 4%	1.00 ± 0.01	u	120 ± 4	± 2.2%	105 ± 6	± 3%

FOV = Field of View; L = linear array probe; P = phased array probe; C = convex array probe. f_h is the maximum harmonic probe frequency; g = gaussian distribution; t = triangular distribution; u = uniform distribution. Results are expressed in terms of mean ± uncertainty (uncertainty δ_{AdSTM} and δ_{NEM} for AdSTM and NEM, respectively). Alongside DOP results, the percentage error values with respect to the FOV are reported and computed as $\delta_{AdSTM\%} = (100 \cdot \delta_{AdSTM} / FOV)$ and $\delta_{NEM\%} = (100 \cdot \delta_{NEM} / FOV)$, respectively; (a) AdSTM does not provide a SNR threshold value when DOP value is greater or equal to the FOV; (b) A no negligible number of tests provided a DOP value above the FOV.

TABLE V

ADSTM AND NEM MEAN PERCENTAGE ERROR FOR EACH US PROBE ACCORDING TOTHE ATTENUATION COEFFICIENT

US probe model	Method	Mean percentage error	
		0.70 dB·cm^{-1}·MHz^{-1}	0.50 dB·cm^{-1}·MHz^{-1}
L	AdSTM	3.2 %	3.2 %
	NEM	3.6 %	3.7 %
P	AdSTM	1.6 %	1.8 %
	NEM	3.7 %	4.9 %
C	AdSTM	1.8 %	2.1 %
	NEM	4.3 %	4.1 %

L = linear array probe; P = phased array probe; C = convex array probe.

shows a lower dispersion as compared to NEM, corroborating the preliminary results found in [19]. In addition, an analysis of the mean percentage error for each US probe model was performed (see Table V). AdSTM showed the lowest mean percentage error (1.6%) with phased array probes at 0.70 dB·cm^{-1}·MHz^{-1}, while NEM displayed its minimum (3.6%) with linear array probes at 0.70 dB·cm^{-1}·MHz^{-1}. AdSTM showed the highest mean percentage error (3.2%) with linear array probes, while NEM showed its maximum (4.9%) with phased array probes at 0.50 dB·cm^{-1}·MHz^{-1}. The linear array probe model showed the lowest observers' mean percentage error.

V. DISCUSSION

In order to perform a compatibility analysis [30], given the low observer population sample involved in this study, a compatibility criterion was used through the application of

TABLE VI
DOP PERCENTAGE DIFFERENCES, BETWEEN ADSTM AND NEM, NORMALIZED WITH RESPECT TO THE FOV FOR BOTH ATTENUATION ZONES FOR ALL THE US SYSTEMS

US system and probe		FOV (mm)	f_{probe}	ΔDOP% 0.70 dB·cm^{-1}·MHz^{-1}	ΔDOP% 0.50 dB·cm^{-1}·MHz^{-1}
Ultrasound System I	L	70	f_{min}	4 ± 5 %	4 ± 4 %
			f_{med}	10 ± 4 %	1 ± 12 %
			f_{max}	0 ± 4 %	—
			f_h	6 ± 4 %	0 ± 4 %
	P	180	f_{min}	8 ± 4 %	—
			f_{med}	6 ± 6 %	—
			f_{max}	Probe frequency not available	
			f_h	7 ± 4 %	—
	C	180	f_{min}	5 ± 5 %	—
			f_{med}	7 ± 5 %	—
			f_{max}	13 ± 3 %	—
			f_h	21 ± 6 %	—
Ultrasound System II	L	70	f_{min}	3 ± 2 %	4 ± 4 %
			f_{med}	0 ± 2 %	3 ± 2 %
			f_{max}	6 ± 2 %	3 ± 2 %
			f_h	7 ± 4 %	6 ± 4 %
	P	180	f_{min}	Data not available	
			f_{med}	1 ± 7 %	5 ± 7 %
			f_{max}	Data not available	
			f_h	7 ± 4 %	1 ± 4 %
	C	180	f_{min}	13 ± 12 %	—
			f_{med}	12 ± 5 %	—
			f_{max}	5 ± 4 %	—
			f_h	18 ± 5 %	6 ± 5 %
Ultrasound System III	L	70	f_{min}	4 ± 4 %	1 ± 5 %
			f_{med}	6 ± 4 %	3 ± 5 %
			f_{max}	7 ± 4 %	3 ± 4 %
			f_h	9 ± 4 %	0 ± 4 %
	P	180	f_{min}	10 ± 4 %	2 ± 6 %
			f_{med}	9 ± 4 %	4 ± 6 %
			f_{max}	13 ± 6 %	1 ± 5 %
			f_h	8 ± 4 %	1 ± 4 %
	C	180	f_{min}	9 ± 4 %	7 ± 4 %
			f_{med}	11 ± 4 %	6 ± 4 %
			f_{max}	8 ± 5 %	6 ± 4 %
			f_h	16 ± 7 %	7 ± 4 %
Ultrasound System IV	L	120	f_{min}	16 ± 8 %	8 ± 3 %
		74	f_{med}	11 ± 5 %	5 ± 6 %
			f_{max}	7 ± 7 %	5 ± 5 %
			f_h	7 ± 4 %	9 ± 5 %
	P	191	f_{min}	2 ± 6 %	—
			f_{med}	9 ± 5 %	7 ± 5 %
			f_{max}	10 ± 5 %	1 ± 7 %
			f_h	13 ± 3 %	13 ± 4 %
	C	184	f_{min}	17 ± 7 %	5 ± 13 %
			f_{med}	20 ± 4 %	15 ± 4 %
			f_{max}	24 ± 6 %	18 ± 6 %
			f_h	24 ± 3 %	11 ± 5 %
Ultrasound System V	L	90	f_{min}	7 ± 4 %	0 ± 5 %
			f_{med}	3 ± 4 %	2 ± 3 %
			f_{max}	2 ± 8 %	3 ± 4 %
			f_h	6 ± 3 %	0 ± 3 %
	P	180	f_{min}	5 ± 2 %	2 ± 4 %
			f_{med}	9 ± 3 %	3 ± 3 %
			f_{max}	7 ± 2 %	4 ± 4 %
			f_h	5 ± 2 %	4 ± 3 %
	C	190	f_{min}	7 ± 5 %	3 ± 4 %
			f_{med}	5 ± 5 %	4 ± 3 %
			f_{max}	6 ± 3 %	6 ± 3 %
			f_h	4 ± 4 %	2 ± 5 %
Ultrasound System VI	L	100	f_{min}	6 ± 4 %	12 ± 8 %
			f_{med}	7 ± 4 %	16 ± 4 %
			f_{max}	2 ± 8 %	7 ± 6 %
			f_h	6 ± 5 %	5 ± 4 %
	P	180	f_{min}	12 ± 3 %	—
			f_{med}	13 ± 4 %	—
			f_{max}	13 ± 3 %	2 ± 15 %
			f_h	9 ± 2 %	11 ± 4 %
	C	180	f_{min}	7 ± 4 %	8 ± 5 %
			f_{med}	12 ± 3 %	6 ± 8 %
			f_{max}	11 ± 4 %	9 ± 7 %
			f_h	8 ± 5 %	8 ± 4 %

L = linear array probe; P = phased array probe; C = convex array probe; f_h is the maximum harmonic probe frequency.

two thresholds, depending on the medium attenuation. First, DOP percentage differences $\Delta\text{DOP}_{\%}$, between the AdSTM and the NEM, normalized to the FOV, were computed (see Table VI), as follows:

$$\Delta\text{DOP}_{\%} = \mu_{\Delta\text{DOP}\%} \pm \delta_{\Delta\text{DOP}\%} \tag{4}$$

where

$$\mu_{\Delta\text{DOP}\%} = \frac{(\mu_{\text{AdSTM}} - \mu_{\text{NEM}})}{\text{FOV}} \cdot 100 \tag{5}$$

$$\delta_{\Delta\text{DOP}\%} = \frac{\sqrt{\left(\delta^2_{\text{AdSTM}} + \delta^2_{\text{NEM}}\right)}}{\text{FOV}} \cdot 100. \tag{6}$$

Afterward, the distributions of $\mu_{\Delta\text{DOP}\%}$ values that are strictly compatible according to [30] were used to determine the maximum acceptable differences between the DOP values, depending on the medium attenuation, $\text{th}_{C,0.70}$ and $\text{th}_{C,0.50}$, as follows:

$$\begin{cases} \text{th}_{C,0.70} = \overline{\mu}_{0.70} + 3\overline{S}_{0.70} \\ \text{th}_{C,0.50} = \overline{\mu}_{0.50} + 3\overline{S}_{0.50} \end{cases} \tag{7}$$

where $\bar{\mu}_{0.70}$ and $\bar{\mu}_{0.50}$ are the mean values of $\mu_{\Delta\text{DOP}\%}$ at 0.70 and 0.50 dB·cm^{-1}·MHz^{-1}, respectively, while $\bar{S}_{0.70}$ and $\bar{S}_{0.50}$ are the corresponding SDs. The values obtained were $\text{th}_{C,0.70} = 13\%$ and $\text{th}_{C,0.50} = 11\%$, respectively. Therefore, all the AdSTM and the NEM DOP measurements from which it resulted that $\Delta\text{DOP}_{\%} \leq \text{th}_C$ for the corresponding attenuation zone, were considered as compatible. Therefore, the percentage of DOP results that showed a significant discrepancy between the AdSTM and the NEM, corresponds to less than 6% for 0.70 dB·cm^{-1}·MHz^{-1} and less than 3%

for 0.50 $dB \cdot cm^{-1} \cdot MHz^{-1}$. These percentages could be due to US images that presented a low dynamic range (darker images), or a higher noise level, in correspondence with the used scanning setting. Hence, it can be assessed that, globally, the two methods applied in this study provide compatible results, at different probe models and operating frequencies, as well as attenuation coefficients.

Finally, it must be pointed out that the values obtained with AdSTM were systematically higher than the NEM ones. This could be related to 1) a higher sensitivity of the automatic method as compared to the human eye, 2) the limited observers' population sample, and/or 3) reduced observers' technical expertise. Anyway, this suggests that the AdSTM may need a calibration procedure to correct for the small bias that systematically affects the DOP measurements. Such a procedure could be based on the SNR threshold assessment on the actual US system dynamic range rather than on the full luminance scale.

VI. Conclusion

In this study, the AdSTM was tested on six intermediate technology-level US diagnostic systems, each of which was equipped with three US probe models, operating at four different frequencies. The measurements were taken with a multi-purpose, multi-tissue US phantom with two different attenuation zones (0.70 and 0.50 $dB \cdot cm^{-1} \cdot MHz^{-1}$). A first series of MCSs was performed for the uncertainty assessment of the SNR thresholds. Then, the outcomes of the first simulations were used in a second series of MCSs to estimate the repeatability DOP uncertainty of the AdSTM. DOP measurements were compared with the mean judgment outcomes of five independent observers, through the NEM implemented with an in-house MATLAB function. One-way ANOVA was performed on NEM uncertainties to check for intra- and inter-observer variability. The obtained results were globally compatible among the methods implied despite the limited observers' population sample. Further investigations could consist in both increasing the observers' population sample size and repeating that with a different population sample with higher technical expertise. Moreover, it would be interesting to develop a calibration procedure for the AdSTM to minimize bias occurring systematically in DOP measurements.

Acknowledgment

The authors would like to thank Jan Galo of the Clinical Engineering Service at IRCCS Children Hospital Bambino Gesù, SIEMENS Healthineers, SAMSUNG Healthcare, PHILIPS Healthcare, HITACHI Healthcare, GE Healthcare, and ESAOTE for hardware supply and technical assistance in data collection.

References

[1] Z. F. Lu, N. J. Hangiandreou, and P. Carson, "Clinical ultrasonography physics: State of practice," in *Clinical Imaging Physics: Current and Emerging Practice*, 1st ed. Hoboken, NJ, USA: Wiley, 2020, pp. 261–286.

[2] N. J. Hangiandreou, S. F. Stekel, D. J. Tradup, K. R. Gorny, and D. M. King, "Four-year experience with a clinical ultrasound quality control program," *Ultrasound Med. Biol.*, vol. 37, no. 8, pp. 1350–1357, Aug. 2011, doi: 10.1016/j.ultrasmedbio.2011.05.007.

[3] S. Balbis, T. Meloni, S. Tofani, F. Zenone, D. Nucera, and C. Guiot, "Criteria and scheduling of quality control of B-mode and Doppler ultrasonography equipment," *J. Clin. Ultrasound*, vol. 40, no. 3, pp. 167–173, Mar./Apr. 2012, doi: 10.1002/jcu.21897.

[4] E. Sassaroli, C. Crake, A. Scorza, D. Kim, and M. Park, "Image quality evaluation of ultrasound imaging systems: Advanced B-modes," *J. Appl. Clin. Med. Phys.*, vol. 20, no. 3, pp. 115–124, Mar. 2019, doi: 10.1002/acm2.12544.

[5] O. Sipilä, V. Mannila, and E. Vartiainen, "Quality assurance in diagnostic ultrasound," *Eur. J. Radiol.*, vol. 80, no. 2, pp. 519–525, Nov. 2011, doi: 10.1016/j.ejrad.2010.11.015.

[6] *Ultrasonics—Pulse-echo scanners—Part 2: Measurement of Maximum Depth of Penetration and Local Dynamic Range*, Standard IEC 61391-2:2010-01, 2011.

[7] N. J. Dudley and N. M. Gibson, "Is grey level a suitable alternative to low-contrast penetration as a serial measure of sensitivity in computerised ultrasound quality assurance?" *Ultrasound Med. Biol.*, vol. 43, no. 2, pp. 541–545, Feb. 2017, doi: 10.1016/j.ultrasmedbio.2016.09.023.

[8] *IPEM Report no 102 Quality Assurance of Ultrasound Imaging Systems*, Inst. Phys. Eng. Med. (IPEM), York, U.K., 2010.

[9] M. M. Goodsitt, P. L. Carson, S. Witt, D. L. Hykes, and J. M. Kofler, "Real-time B-mode ultrasound quality control test procedures. Report of AAPM ultrasound task group, no. 1," *Med. Phys.*, vol. 25, no. 8, pp. 1385–1406, Oct. 1998, doi: 10.1118/1.598404.

[10] American Institute of Ultrasound in Medicine (AIUM). *AIUM Routine Quality Assurance of Clinical Ultrasound Equipment, Version 2.0*. Accessed: Feb. 4, 2023. [Online]. Available: http://aium.s3.amazonaws.com/resourceLibrary/rqa2.pdf

[11] *AIUM Quality Assurance Manual for Gray Scale Ultrasound Scanners*, Amer. Inst. Ultrasound Med. (AIUM), Laurel, MD, USA, 2014.

[12] N. M. Gibson, N. J. Dudley, and K. Griffith, "A computerised quality control testing system for B-mode ultrasound," *Ultrasound Med. Biol.*, vol. 27, no. 12, pp. 1697–1711, Dec. 2001, doi: 10.1016/s0301-5629(01)00479-3.

[13] J. M. Thijssen, G. Weijers, and C. L. de Korte, "Objective performance testing and quality assurance of medical ultrasound equipment," *Ultrasound Med. Biol.*, vol. 33, no. 3, pp. 460–471, Mar. 2007, doi: 10.1016/j.ultrasmedbio.2006.09.006.

[14] A. Scorza, G. Lupi, S. A. Sciuto, F. Bini, and F. Marinozzi, "A novel approach to a phantom based method for maximum depth of penetration measurement in diagnostic ultrasound: A preliminary study," in *Proc. IEEE Int. Symp. Med. Meas. Appl. (MeMeA)*, Turin, Italy, May 2015, pp. 369–374, doi: 10.1109/MeMeA.2015.7145230.

[15] K. R. Gorny, D. J. Tradup, and N. J. Hangiandreou, "Implementation and validation of three automated methods for measuring ultrasound maximum depth of penetration: Application to ultrasound quality control," *Med. Phys.*, vol. 32, no. 8, pp. 2615–2628, Aug. 2005, doi: 10.1118/1.1951095.

[16] C. Kollmann, C. deKorte, N. Dudley, N. Gritzmann, K. Martin, and D. Evans, "Guideline for technical quality assurance (TQA) of ultrasound devices (B-mode)—version 1.0 (July 2012)," *Ultraschall der Medizin*, vol. 33, no. 06, pp. 544–549, Nov. 2012, doi: 10.1055/s-0032-1325347.

[17] E. Sassaroli, A. Scorza, C. Crake, S. A. Sciuto, and M.-A. Park, "Breast ultrasound technology and performance evaluation of ultrasound equipment: B-mode," *IEEE Trans. Ultrason., Ferroelectr., Freq., Control*, vol. 64, no. 1, pp. 192–205, Jan. 2017, doi: 10.1109/tuffc.2016.2619622.

[18] N. Dudley and N. Gibson, "Early experience with automated B-mode quality assurance tests," *Ultrasound*, vol. 22, no. 1, pp. 15–20, Feb. 2014, doi: 10.1177/1742271x13516896.

[19] G. Fiori, F. Fuiano, A. Scorza, J. Galo, S. Conforto, and S. A. Sciuto, "A preliminary study on the adaptive SNR threshold method for depth of penetration measurements in diagnostic ultrasounds," *Appl. Sci.*, vol. 10, no. 18, p. 6533, Sep. 2020, doi: 10.3390/app10186533.

[20] G. Fiori et al., "A preliminary study on a novel method for depth of penetration measurement in ultrasound quality assessment," in *Proc. 24th IMEKO TC4 Int. Symp. 22nd Int. Workshop ADC Modelling Test.*, Palermo, Italy, 2020, pp. 332–336. [Online]. Available: https://www.imeko.org/publications/tc4-2020/IMEKO-TC4-2020-62.pdf

[21] T. Kimpe and T. Tuytschaever, "Increasing the number of gray shades in medical display systems—How much is enough?" *J. Digit. Imag.*, vol. 20, no. 4, pp. 422–432, Dec. 2007, doi: 10.1007/s10278-006-1052-3.

[22] G. Fiori, A. Scorza, M. Schmid, J. Galo, S. Conforto, and S. A. Sciuto, "A preliminary study on the blind angle estimation for quality assessment of color Doppler ultrasound diagnostic system," in *Proc. 25th IMEKO TC4 Int. Symp. 23rd Int. Workshop ADC DAC Modelling Test.*, Brescia, Italy, 2022, pp. 12–14.

[23] *CIRS Tissue Simulation & Phantom Technology, Multi-Purpose, Multi-Tissue Ultrasound Phantom—Model 040GSE*. Accessed: Feb. 4, 2023. [Online]. Available: http://www.cirsinc.com/wp-content/uploads/2020/03/040GSE-DS-032320-1.pdf

[24] *Evaluation of Measurement Data—Supplement 1 to the 'Guide to the Expression of Uncertainty in Measurement'—Propagation of Distributions Using a Monte Carlo Method*, document JCGM 101:2008, 2008. [Online]. Available: https://www.bipm.org/documents/20126/2071204/JCGM_101_2008_E.pdf/325dcaad-c15a-407c-1105-8b7f322d651c

[25] G. Fiori, F. Fuiano, A. Scorza, J. Galo, S. Conforto, and S. A. Sciuto, "A preliminary study on an image analysis based method for lowest detectable signal measurements in pulsed wave Doppler ultrasounds," *Acta IMEKO*, vol. 10, no. 2, pp. 126–132, Jun. 2021, doi: 10.21014/acta_imeko.v10i2.1051.

[26] F. Vurchio, G. Fiori, A. Scorza, and S. A. Sciuto, "Comparative evaluation of three image analysis methods for angular displacement measurement in a MEMS microgripper prototype: A preliminary study," *Acta IMEKO*, vol. 10, no. 2, pp. 119–125, Jun. 2021, doi: 10.21014/acta_imeko.v10i2.1047.

[27] F. Vurchio, G. Bocchetta, G. Fiori, A. Scorza, N. P. Belfiore, and S. A. Sciuto, "A preliminary study on the dynamic characterization of a MEMS microgripper for biomedical applications," in *Proc. IEEE Int. Symp. Med. Meas. Appl. (MeMeA)*, Lausanne, Switzerland, Jun. 2021, pp. 1–6, doi: 10.1109/MeMeA52024.2021.9478703.

[28] G. Fiori, A. Scorza, M. Schmid, J. Galo, S. Conforto, and S. A. Sciuto, "A novel method for the gain conversion factor estimation in quality assessment of ultrasound diagnostic systems," in *Proc. IEEE Int. Symp. Med. Meas. Appl. (MeMeA)*, Messina, Italy, Jun. 2022, pp. 1–5, doi: 10.1109/MeMeA54994.2022.9856491.

[29] A. Scorza, S. Conforto, C. D'Anna, and S. A. Sciuto, "A comparative study on the influence of probe placement on quality assurance measurements in B-mode ultrasound by means of ultrasound phantoms," *Open Biomed. Eng. J.*, vol. 9, no. 1, pp. 164–178, Jul. 2015, doi: 10.2174/1874120701509010164.

[30] J. R. Taylor, *An Introduction to Error Analysis: The Study of Uncertainties in Physical Measurements*. Sausalito, CA, USA: Univ. Science Books, 1996, pp. 245–260.

Giorgia Fiori (Member, IEEE) received the bachelor's degree in electronic engineering and the master's degree in biomedical engineering from Roma Tre University, Rome, Italy, in 2016 and 2019, respectively, where she is currently pursuing the Ph.D. degree in applied electronics with the Department of Industrial, Electronic and Mechanical Engineering.

Her research interests include clinical engineering, mechanical and thermal measurement systems and instrumentation, as well as methods and systems for quality assessment of Doppler ultrasound equipment for clinical use.

Fabio Fuiano received the bachelor's degree in electronic engineering and the master's degree in biomedical engineering from Roma Tre University, Rome, Italy, in 2016 and 2019, respectively, where he is currently pursuing the Ph.D. degree in mechanical and industrial engineering with the Department of Industrial, Electronic and Mechanical Engineering.

His research interests include methods for the quantitative evaluation of blood vessel stiffness based on ultrasound measurements.

Maurizio Schmid (Senior Member, IEEE) received the Ph.D. degree in biomedical engineering from the University of Bologna, Bologna, Italy, in 2004.

He is currently a Full Professor in biomedical engineering with the Department of Industrial, Electronic and Mechanical Engineering, Roma Tre University, Rome, Italy, where he directs BioLab^3—the Laboratory of Biomedical Engineering. His research interests include the development of device algorithms and classification methods in the area of human movement analysis, where he is now involved in studies on the use of inertial sensors as tools for disease staging and ambient assisted living.

Silvia Conforto (Member, IEEE) received the Electronic Engineering and Ph.D. degrees in biomedical engineering from the Sapienza University of Rome, Rome, Italy, in 1992 and 1999, respectively.

She is currently a Full Professor of bioengineering with the Department of Industrial, Electronic and Mechanical Engineering, Roma Tre University, Rome. Her current research interests include biosignal processing, pattern recognition, neural networks, and human motion analysis.

Salvatore A. Sciuto (Member, IEEE) is currently a Full Professor of measurements and clinical engineering with the Department of Industrial, Electronic, and Mechanical Engineering, Roma Tre University, Rome, Italy. His current research interests include sensors for health devices, neonatal mechanical ventilation, noninvasive medical measurements, QC of biomedical instrumentation, HTA, and clinical engineering.

Andrea Scorza received the Ph.D. degree in mechanical measurement for engineering from the University of Padua, Padua, Italy, in 2004.

He is currently an Associate Professor of measurements and clinical engineering with the Department of Industrial, Electronic and Mechanical Engineering, Roma Tre University, Rome, Italy. His research interests include mechanical and thermal measurement systems and instrumentation, design, and testing of biomedical instrumentation, and experimental mechanics applied in the biomedical field.

Open Access funding provided by 'Università degli Studi Roma Tre' within the CRUI CARE Agreement